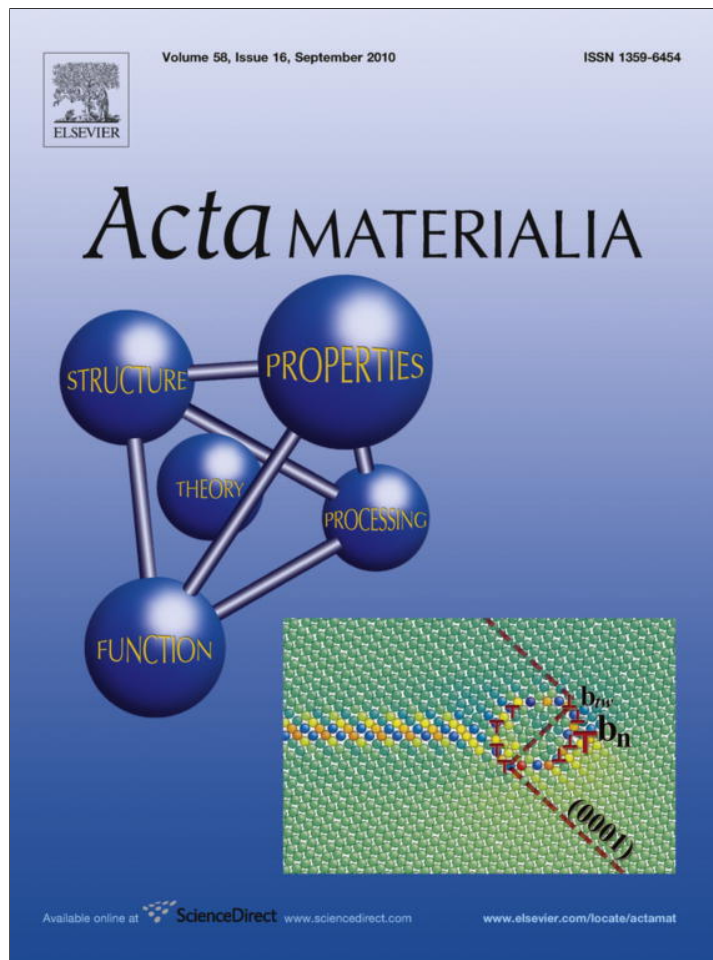


Provided for non-commercial research and education use.  
Not for reproduction, distribution or commercial use.



This article appeared in a journal published by Elsevier. The attached copy is furnished to the author for internal non-commercial research and education use, including for instruction at the authors institution and sharing with colleagues.

Other uses, including reproduction and distribution, or selling or licensing copies, or posting to personal, institutional or third party websites are prohibited.

In most cases authors are permitted to post their version of the article (e.g. in Word or Tex form) to their personal website or institutional repository. Authors requiring further information regarding Elsevier's archiving and manuscript policies are encouraged to visit:

<http://www.elsevier.com/copyright>

# Report Documentation Page

Form Approved  
OMB No. 0704-0188

Public reporting burden for the collection of information is estimated to average 1 hour per response, including the time for reviewing instructions, searching existing data sources, gathering and maintaining the data needed, and completing and reviewing the collection of information. Send comments regarding this burden estimate or any other aspect of this collection of information, including suggestions for reducing this burden, to Washington Headquarters Services, Directorate for Information Operations and Reports, 1215 Jefferson Davis Highway, Suite 1204, Arlington VA 22202-4302. Respondents should be aware that notwithstanding any other provision of law, no person shall be subject to a penalty for failing to comply with a collection of information if it does not display a currently valid OMB control number.

1. REPORT DATE <b>15 JUN 2010</b>		2. REPORT TYPE		3. DATES COVERED <b>00-00-2010 to 00-00-2010</b>	
4. TITLE AND SUBTITLE <b>Three-dimensional analysis of grain topology and interface curvature in a b-titanium alloy</b>				5a. CONTRACT NUMBER	
				5b. GRANT NUMBER	
				5c. PROGRAM ELEMENT NUMBER	
6. AUTHOR(S)				5d. PROJECT NUMBER	
				5e. TASK NUMBER	
				5f. WORK UNIT NUMBER	
7. PERFORMING ORGANIZATION NAME(S) AND ADDRESS(ES) <b>U. S. Naval Research Laboratory, Code 6350, 4555 Overlook Ave. SW, Washington, DC, 20375-4000</b>				8. PERFORMING ORGANIZATION REPORT NUMBER	
9. SPONSORING/MONITORING AGENCY NAME(S) AND ADDRESS(ES)				10. SPONSOR/MONITOR'S ACRONYM(S)	
				11. SPONSOR/MONITOR'S REPORT NUMBER(S)	
12. DISTRIBUTION/AVAILABILITY STATEMENT <b>Approved for public release; distribution unlimited</b>					
13. SUPPLEMENTARY NOTES					
14. ABSTRACT <b>While considerable efforts have been made to model the effects of grain coarsening, there has been little experimental verification of these models. Using serial sectioning techniques, the full 3-D morphology of 2098 b-titanium grains in Ti-21S are analyzed and directly compared to grain coarsening theories. The experimental grain size distribution and the distribution in the number of grain faces are shown to have a close comparison to the predictions of the steady-state size distribution from a number of simulations and analytical theories. The geometric factor of the growth rates is determined by measuring the mean curvature of the grain faces. It is found that, on average, the grains with an average of 15.5 faces have a zero integral mean curvature of the grain faces, higher than the predicted value of 13.4 faces. This difference is suggested to be due to the non-random nearest-neighbor effects within the grain network.</b>					
15. SUBJECT TERMS					
16. SECURITY CLASSIFICATION OF:			17. LIMITATION OF ABSTRACT	18. NUMBER OF PAGES	19a. NAME OF RESPONSIBLE PERSON
a. REPORT <b>unclassified</b>	b. ABSTRACT <b>unclassified</b>	c. THIS PAGE <b>unclassified</b>			



# Three-dimensional analysis of grain topology and interface curvature in a $\beta$ -titanium alloy

D.J. Rowenhorst\*, A.C. Lewis, G. Spanos

*U. S. Naval Research Laboratory, Code 6350, 4555 Overlook Ave. SW, Washington, DC 20375-4000, USA*

Received 14 April 2010; received in revised form 15 June 2010; accepted 16 June 2010  
Available online 14 July 2010

## Abstract

While considerable efforts have been made to model the effects of grain coarsening, there has been little experimental verification of these models. Using serial sectioning techniques, the full 3-D morphology of 2098  $\beta$ -titanium grains in Ti–21S are analyzed and directly compared to grain coarsening theories. The experimental grain size distribution and the distribution in the number of grain faces are shown to have a close comparison to the predictions of the steady-state size distribution from a number of simulations and analytical theories. The geometric factor of the growth rates is determined by measuring the mean curvature of the grain faces. It is found that, on average, the grains with an average of 15.5 faces have a zero integral mean curvature of the grain faces, higher than the predicted value of 13.4 faces. This difference is suggested to be due to the non-random nearest-neighbor effects within the grain network. Published by Elsevier Ltd. on behalf of Acta Materialia Inc.

*Keywords:* 3-D serial sectioning; Grain growth; Grain morphology

## 1. Introduction

One of the more commonly observed microstructures is the arrangement of single-phase polycrystalline grains forming a network of irregular polyhedra. At elevated temperatures, the arrangement of grains will evolve such that the average grain size increases, leading to a decrease in the total interfacial area of the system, a process commonly referred to as grain coarsening. Understanding the structure and evolution of grain networks is critical for a wide array of materials science problems, including the evolution of grain interfacial textures, phase transformations and prediction of materials properties at elevated temperatures. Furthermore, similar space-filling cellular network structures are found in other scientific disciplines including gas–liquid foams and biological cells.

While there have been many theories and simulations formulated to predict the evolution of the microstructure during grain coarsening [1–12], there have been very few

experimental verifications of these phenomena, and existing information has been based almost exclusively on experimental data gathered from individual two-dimensional (2-D) cross-sections [13,14]. While some statistical comparisons can be made using 2-D stereological techniques, direct determination of grain topology and interface curvatures requires knowledge of the 3-D morphology of the grains in the structure.

Some of the earliest work applying space-filling grain structures to solid materials systems was by Smith [1,15,16]. Later Mullins and von Neumann [2,3] showed that the evolution of the grain boundary interfaces is proportional to the local mean curvature for that interface, and thus the total growth rate of the grain,  $\frac{dV}{dt}$ , is given by

$$\frac{dV}{dt} = -M\gamma\mathcal{H} \quad (1a)$$

$$\mathcal{H} = \int_{\text{Faces}} \left( \frac{1}{R_1} + \frac{1}{R_2} \right) dS \quad (1b)$$

where  $M$  is a mobility constant for the grain interface,  $\gamma$  is the interface energy and  $\mathcal{H}$  is the integral mean curvature of the grain faces, defined in Eq. (1b), where  $R_1$  and  $R_2$

\* Corresponding author. Tel.: +1 202 767 2565; fax: +1 202 767 2623.  
E-mail address: [david.rowenhorst@nrl.navy.mil](mailto:david.rowenhorst@nrl.navy.mil) (D.J. Rowenhorst).

are the principal curvatures of a small patch with area  $S$ , summed over all of the grain faces (thus excluding curvature at the triple lines). This is often normalized by the grain size by:

$$\frac{dV}{dt} \frac{1}{V^{1/3}} = M\gamma\mathcal{G} \quad (2)$$

where  $\mathcal{G}$  represents the normalized integral mean curvature of the grain faces, and is related to the growth rate of the grain. Von Neumann showed that in two dimensions the integral mean curvature of area-filling grains can be completely determined by counting the number of faces of a grain, and that grains with more than six faces will have a positive growth rate, grains with fewer than six faces have a negative growth rate, and those grains comprising exactly six faces in two dimensions have a zero growth rate and will not grow or shrink until they undergo a topological change.

The relationship between the grain shape and its growth rate in three dimensions is considerably more complicated than in the 2-D case due to the extra degree of freedom in three dimensions, and thus it cannot be determined solely by the number of grain faces. For 3-D systems, Cahn [4] showed that the integral mean curvature of convex bodies is related to the mean caliper diameter of that body. More recently, this was generalized by MacPherson and Srolovitz [11] for all closed bodies, where the normalized growth rate of a grain is related by:

$$\mathcal{G} = \frac{1}{V^{1/3}} \left( 2\pi\mathcal{L} - \frac{2\pi}{6} \sum_{i=1}^n e_i \right) \quad (3)$$

where  $\mathcal{L}$  is the mean width of the grain and  $\sum_{i=1}^n e_i$  is the summation of the triple line lengths,  $e$ , of the grain. The mean width is related to the integral mean curvature by the simple relation,  $\mathcal{H} = 2\pi\mathcal{L}$ . The term  $\frac{2\pi}{6} \sum_{i=1}^n e_i$  describes the total curvature of the triple lines for the grain, assuming that the triple lines have the ideal dihedral angle of  $2\pi/3$ . This then provides an exact solution for the evolution of individual grains within the network; however, it does not describe the average behavior of the grain network as a whole.

In order to directly compare to these theories, the full 3-D structure of the grains needs to be determined. In large part due to recent developments in 3-D experimental and quantitative analysis techniques [17–19], it has recently become feasible to make measurements in three dimensions for relatively large ensembles of grains ( $\geq 1000$  grains) in solids [20,21]. In this work, we have employed serial sectioning to reconstruct the grain shapes of 2098  $\beta$  grains in a titanium alloy and make direct comparisons to these theories. The grain size, interface curvature and number of grain faces of each grain is measured directly, and these results are compared to current theories of 3-D grain evolution. The results show the importance of considering not only the average grain topology, but also the topology of the nearest grain neighbors.

## 2. Procedure

Serial sectioning was used to measure the 3-D microstructure of Ti–21S, a  $\beta$ -stabilized titanium alloy provided by TiMet Corp, with a composition of Ti–15.4Mo–2.9Nb–2.9Al–0.17Si–0.29Fe–0.12O. As received from TiMet, the alloy was fully recrystallized and annealed at 843 °C for 20 min, providing a uniform equiaxed grain structure with a mean grain diameter of 39  $\mu\text{m}$ . To verify that the microstructure was near a steady-state condition, the as-received material was heated at 830 °C for 4 and 12 h, leading to a 2-D average grain diameter of 53.6 and 121.6  $\mu\text{m}$ , respectively. Two-dimensional analysis of the grain size distribution normalized to the average grain size showed that it was self-similar with the as-received sample. To maximize the number of grains in the serial sectioning volume, the as-received material was used in the serial sectioning analysis.

The removal of material between each section was performed by a Struers TegraPol semi-automatic polisher, which applies a constant pressure to the sample on the polishing cloth for a fixed amount of time, providing a reliable material removal rate for each section. The polishing was accomplished using a two-step polish. In the first step, the specimen was polished for 2 min using 3  $\mu\text{m}$  diamond slurry to remove the majority of the material. The second step used a 0.04  $\mu\text{m}$  silica slurry, which provides a final surface finish appropriate for the optical micrographs. Using this method, 200 optical micrograph sections were collected, with a mean section spacing of 1.48  $\mu\text{m}$ , which provided approximately 25 sections per average-sized grain.

To measure the geometry of the grain interfaces accurately, it was necessary to collect 2-D images that maintained a high image resolution while still containing a large number of grains within the field of view. Thus a montage of  $8 \times 5$  optical micrograph images (using a total objective magnification of  $\times 500$ , with an optical resolution of  $\sim 0.45 \mu\text{m}$ ) was collected for each section using a Zeiss AxioVert Optical Microscope. Each image overlapped its neighboring images, allowing for the images to be stitched together to form one seamless image that was approximately  $1000 \mu\text{m} \times 550 \mu\text{m}$  for each section. The contrast at the grain boundaries was greatly enhanced by precipitation of  $\alpha$ -Ti at the grain boundaries prior to sectioning, which was achieved by heat treatment at 725 °C for 15 min. The  $\alpha$ -Ti was then easily etched using Krohl's etchant, providing the necessary contrast in the optical images. The  $\alpha$ -Ti precipitation did not detectably change the shape of the grain boundaries, thus the  $\alpha$  acts purely as a decoration for the grain boundaries and it does not affect grain topology.

To create the image stack, the sections must be aligned with each other. A coarse scale, long-range image alignment was performed, following a similar technique to Wall et al. [22]. A geometric pattern was etched into the side of the sample, perpendicular to the sectioning plane. In this instance, a series of  $10 \times 10 \mu\text{m}$  channels were etched into

the side of the sample using a Focused Ion Beam (FIB) (FEI Nova 600 DBFIB) before serial sectioning. These channels are revealed at the edge of the sample in cross-section [23]. Channels parallel with the sectioning direction provided fiducial marks for aligning the images, while channels at a known angle from the sectioning direction provided a section-by-section depth calibration. When viewed from the sectioning plane, the cross-section of the channels can be observed at the edge of the sample, providing a long-range alignment of the images so that the first image can be directly aligned with the last image in the serial sectioning stack.

After the images were aligned, the individual grains were segmented within the images so that each grain had a unique identifier associated with it. The first step in this process was to identify the grain boundaries within each 2-D section. The identification of the grain boundaries was performed by thresholding the brightness values of each image so that all the  $\alpha$ -Ti is white and all the  $\beta$ -Ti grains are black. Not all of the grain boundaries are fully coated with  $\alpha$ , leaving some gaps in the grain boundary interfaces within the images. Additionally, some  $\alpha$  precipitated within the  $\beta$  grains. The majority of intragranular  $\alpha$  was removed automatically by using a size rank filter, eliminating any white region that was significantly smaller than the grain boundary network in the image, and any remaining artifacts were removed by manual image processing.

The gaps in the grain boundaries were filled using a watershed segmentation algorithm which also labels each of the grains with a unique identifier. A similar process was used in prior work to automatically segment particle boundaries in a two-phase system [24]. Using this method, a 3-D Euclidian distance function is applied to the stack of images, which labels each voxel in the image with the negative of the minimum distance from that point to the nearest interface, thus the centers of grains become minima within the image. Here an algorithm was used that allows for the non-cuboidal voxels present in this serial sectioning data [25]. The distance function of the 3-D stack is then processed by a 3-D watershed algorithm which labels each

grain uniquely and fills in any missing gaps in the grain boundary network [26]. Because the grains are typically not perfectly equiaxed, a watershed segmentation will often over-segment the structure, placing more boundaries in the image than are actually present. Here this artifact was corrected by using the methodology described by Rowenhorst et al. [24], wherein the local minima in the Euclidian distance map (which should approximate the grain centers) are used to make an estimate of the grain size. Any boundaries that occur within the radius from the grain center have a high probability of being false, and therefore are removed. Further details are provided in the work cited above.

A final sub-pixel alignment of the images was achieved by minimizing the net movement of the area centers of each grain from section to section, similar to the procedure outlined by Rohrer et al. [27]. Because the fiducial marks allow for alignment of the first section with the last, any long-range drift in the sub-pixel alignment was removed by subtracting a linear interpolation of net translations through the stack.

### 3. Results and discussion

#### 3.1. Statistical distributions

Fig. 1 shows the final 3-D reconstructions of the Ti- $\beta$  grain structure, with over 4300 grains within the dataset. Fig. 1a shows the reconstruction of the grains within the region of interest with some of the outside grains removed to reveal the internal grain structure. The grains near the boundary of the analysis volume must be removed in an unbiased fashion. Simply removing any grain that intersects the edge of the volume would preferentially remove large grains, since large grains have a larger surface area and thus have a higher probability of intersecting the boundaries of the reconstructed volume. Therefore any grain was removed whose center of mass lies within a distance of  $2\langle R \rangle$  from the edge of the reconstructed volume, where  $\langle R \rangle$  is the mean grain radius, 19.5  $\mu\text{m}$ . Because the

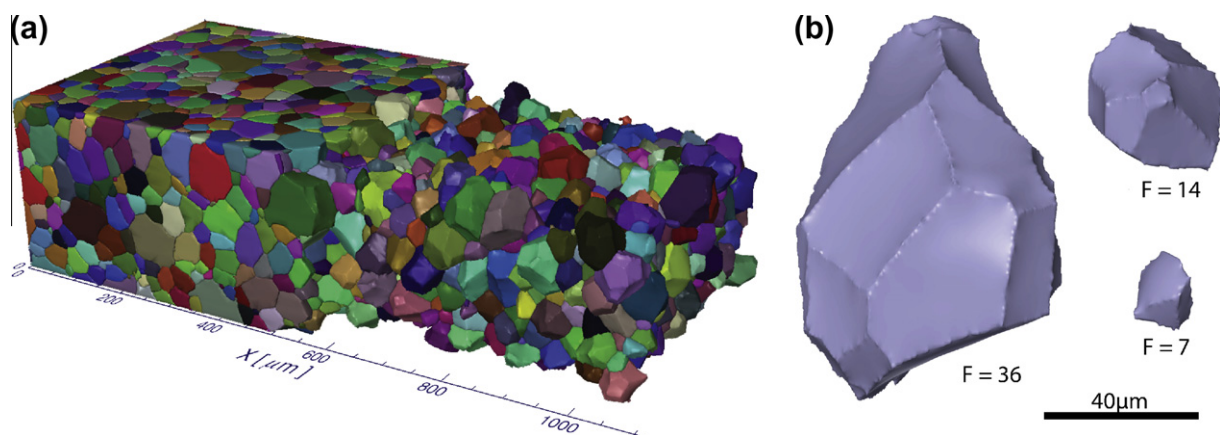


Fig. 1. (a) Reconstruction of 4380  $\beta$  grains from 200 serial sections, of which 2098 grains were analyzed. The entire reconstructed volume is  $1115 \times 516 \times 300 \mu\text{m}^3$ . (b) Sampling of individual grains with varying topology and size. As expected, larger grains tend to have more grain faces.

center of mass does not depend on the size of the grain, this approach avoids preferential selection and removal of large grains from the set being analyzed. This left 2098 grains in the unbiased data set.

Fig. 1b shows the reconstructions of a selection of grains in the structure with varying sizes and numbers of faces, illustrating the expected trend that larger grains tend to have more faces than smaller grains. This is shown clearly in Fig. 2, where the spherical equivalent grain radius is plotted as a function of the number of faces of the grain. The grain radius is determined by measuring the volume of each grain by counting the number of voxels associated with that grain. The number of grain faces in the experiment was determined by counting the number of grains that were direct nearest-neighbors with the voxels that described the central grain, not including the diagonal pixels (though testing showed no significant difference between including or excluding the diagonal voxel neighbors). Fig. 2 shows that for each number of faces there is a distribution of grain sizes, which remains constant at about  $\pm 5 \mu\text{m}$  (ignoring face classes that contain a small number of grains).

The Grain Size Distribution (GSD) of the Ti- $\beta$  grains is shown in Fig. 3, where the spherical equivalent grain radius has been normalized to the mean radius so that it can be directly compared to other grain growth simulations, including the results from a Surface Evolver simulation [6], a phase-field simulation [8] and a Monte Carlo simulation [28]. Additionally, the analytical result from Pande and McFadden is presented (the value of the stochastic variable  $\alpha = 5$  was used as it provided the best fit to the distribution) [29]. Overall it is seen that all the simulations match the shape of the experimental distribution very well. The tails of the distribution are well described by the analytical

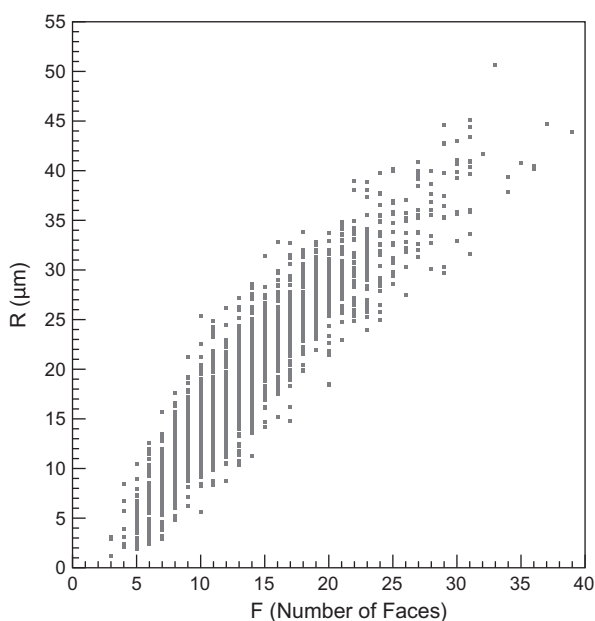


Fig. 2. The spherical equivalent radius,  $R$  vs. the number of grain faces,  $F$ .

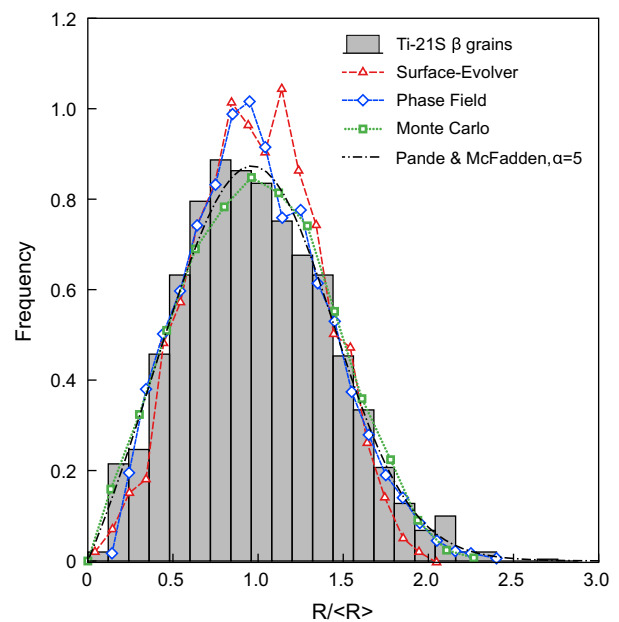


Fig. 3. The spherical equivalent radius grain size distribution normalized by the average grain size. The results from a Surface Evolver simulation [6], a phase-field simulation [8] a Monte Carlo simulation [28] and an analytical theory [29] are plotted for comparison.

theory, as well as the Monte Carlo simulation and the phase-field simulation. The distribution from the Surface Evolver is somewhat noisier and there is some disagreement especially in the tail of the distribution at larger grain sizes. This is most likely due to the small number of grains in that simulation, especially when compared to the size of the simulation domain, thereby introducing boundary effects in the simulation that could significantly affect the statistical representation of the structure.

Fig. 4 plots the distribution in the number of grain faces for each grain. The average number of faces for the system was found to be  $\bar{F} = 13.7$ , which is very close to the average number of grain faces in the simulations ( $\bar{F} = 13.7$  for the phase-field simulation and 13.5 for the Surface Evolver). Also, the distribution in the number of grain faces compares very well to these simulations. At the larger number of faces there is again a discrepancy between the Surface Evolver simulation and the experimentally measured data. It should be noted that the Surface Evolver simulation contained no grains with more than 30 faces while the maximum in the experimental data is 40 faces, and in the phase-field simulation, where a larger number of grains are used, the maximum number of faces is 39. This, then, further suggests that the Surface Evolver simulation did not contain enough grains to be representative of an infinite sample. The Surface Evolver simulation, however, is one of the few simulations that quantify the nearest-neighbor topological interactions (which will be shown to be important for understanding the evolution of the structure), and thus the results are useful for comparison with the experimental results presented here.

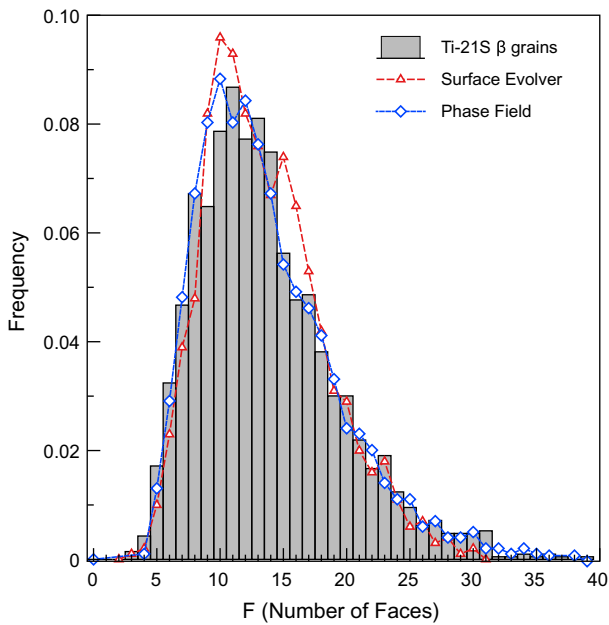


Fig. 4. Distribution in the number of faces per grain. The results from a Surface Evolver simulation [6] and a phase-field simulation [8] are plotted for comparison.

### 3.2. Grain boundary interface curvature

The normalized growth rate,  $\mathcal{G}$ , of a grain can be calculated from the geometry of the surface of the grain. The visualizations of the grain shapes (shown in Fig. 1) represent the grains as discretized triangulated surface meshes, wherein the interface of the grain is described as a set of vertex points, whose connectivity is described by a set of triangles. The creation of the surface mesh is a critical step in not only the visualization of the microstructure but also the analysis. Note that in this article we will refer to the geometric features of the grains as grain faces, triple lines and quadruple points, and the features of the surface mesh as triangles, edges and vertex points.

Since, as far as we are aware, grain face curvatures in a 3-D randomly packed network of grains have not been previously measured, it is important to provide some details as to how these measurements were made. The most common technique to convert a set of regularly gridded voxels (such as a stack of images produced by serial sectioning) to a surface mesh for computer-aided visualization is the Fast Marching Cubes (FMC) algorithm [30]. In this instance, as each point on the interface is shared between two or more grains, an implementation of the Multiple Material Fast Marching Cubes (MM-FMC) algorithm [31] was employed. The MM-FMC algorithm has the distinct advantage of maintaining the shared interfaces between the grains and tracking the number of grains that connect to each vertex point, thereby easily identifying the location of the triple lines within the surface mesh. Fig. 5a shows the results of the MM-FMC for one of the grains, with the identified triple lines labeled in black.

As can be seen in Fig. 5a, one characteristic of FMC algorithms on discrete structures is that the algorithm produces artifacts at the interface that create a stair-stepped surface. To remove these artifacts, a Constrained Laplacian Mesh Smoothing algorithm was implemented. In a traditional Laplacian mesh smoothing, the position of vertex  $i$  is given by  $v_i$  and the new position,  $v'_i$  is given by

$$v'_i = v_i + \frac{\lambda}{N} \sum_{j=1}^N v_j - v_i \quad (4)$$

where  $v_j$  are the locations of the vertices that connect to  $v_i$ ,  $N$  is the number of connected vertices and  $\lambda$  is a weighting factor, typically on the order of 0.1. This, then, is iterated until the desired amount of smoothing is achieved (on the order of 200 iterations). Fig. 5b shows the result of smoothing the surface mesh without any constraint on the mesh points. It is clear from the reconstruction that while the algorithm has removed the artifacts from the FMC, the curvature near the triple junctions and the faces has been

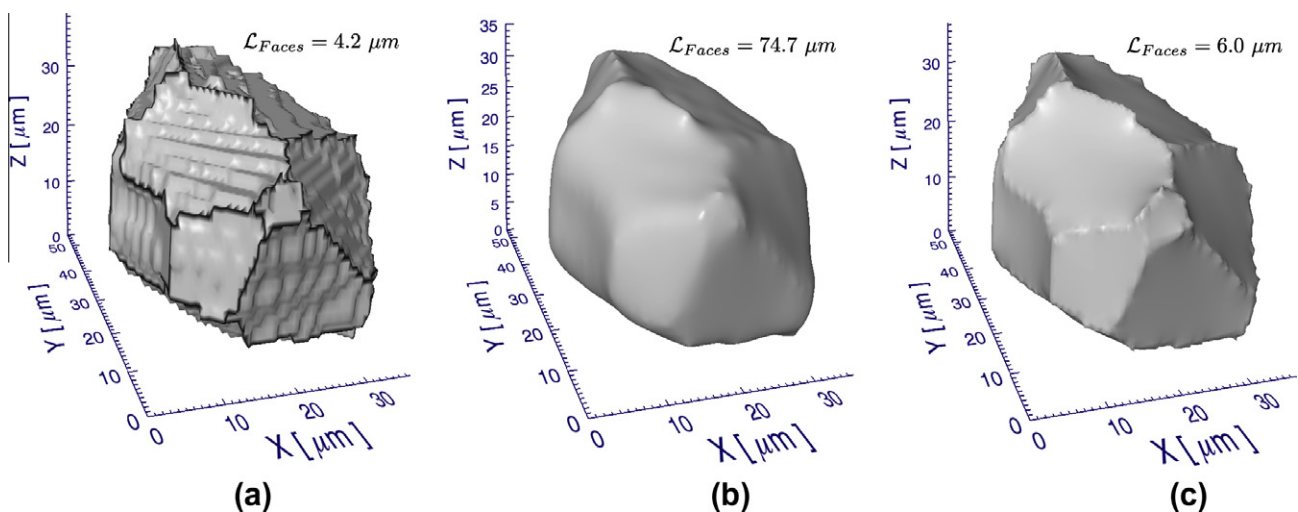


Fig. 5. (a) The as-meshed grain structure. Black lines show the triple lines. (b) Smoothed mesh after 200 iterations with no constraint on the mesh points. (c) Smoothed mesh, constraining the triple lines and a revolving set of randomly chosen constrained points on the grain faces after 200 iterations.

significantly compromised. This is further shown by the drastic change of the measured mean width from 4.2 μm to 74.7 μm.

The desired result is to reduce the local curvature on the grain faces while maintaining the sharpness of the triple junction lines, as well as maintaining the long-range curvature of the faces; thus, a constrained Laplacian smoothing technique is used. Here, 90% of the vertex points in the surface mesh that are shared by three or more regions (i.e. the triple lines in the structure) are fixed in their original locations. In addition, a randomly selected set of vertex points within the grain face (i.e. those that are shared by only two regions) are also fixed. The random vertex points comprise 10% of the vertex points on the grain faces. For each iteration of the Laplacian smoothing, a new set of the random constrained points is chosen. The result of this procedure is shown in Fig. 5c, where it is clear that triple junctions are preserved, and the local high curvature areas on the faces of the grains are eliminated.

For each reconstructed grain in the unbiased volume, the normalized integral mean curvature of the grain faces,  $\mathcal{G}$ , was calculated using a modification of that outlined by MacPherson and Srolovitz [11], wherein the mean width,  $\mathcal{L}$  is given by:

$$\mathcal{L} = \frac{1}{2\pi} \sum_{i=1}^m \epsilon_i \beta_i \quad (5)$$

where  $\epsilon_i$  is the length of the  $i^{\text{th}}$  triangle edge and  $\beta_i$  is the outside turning angle between the two triangles in the surface mesh that contains  $m$  triangle edges [11]. Because the MS-FMC algorithm clearly delineates the edges of the surface mesh that are shared between three regions (i.e. at the triple junctions of the grains,  $\epsilon^{\text{TJ}}$ ) and those triangle edges of the surface mesh that are shared between only two regions (the grain faces,  $\epsilon^{\text{F}}$ ), we can write Eq. (5) as:

$$\mathcal{L} = \frac{1}{2\pi} \left( \sum_{i=1}^{m^{\text{F}}} \epsilon_i^{\text{F}} \beta_i^{\text{F}} + \sum_{j=1}^{m^{\text{TJ}}} \epsilon_j^{\text{TJ}} \beta_j^{\text{TJ}} \right) \quad (6)$$

Substituting this for  $\mathcal{L}$  in Eq. (3), we see that the second summation of Eq. (6) is exactly equivalent to the triple-junction length term of Eq. (3) if one assumes that the turning angles of all the triple lines are 60°. If this simplification is removed and the exact triple-junction turning angle is used for each triple junction, Eq. (3) can be rewritten as:

$$\mathcal{G} = \frac{1}{V^{1/3}} \left( \sum_{i=1}^{m^{\text{F}}} \epsilon_i^{\text{F}} \beta_i^{\text{F}} \right) \quad (7)$$

thus providing  $\mathcal{G}$  without assumption of the triple-junction geometry by only including those edges within the surface mesh of the grains that belong only to the faces of the grains. This methodology has the distinct advantage of not requiring detailed knowledge of the triple-junction geometry, which others have shown can make the measurement of  $\mathcal{G}$  problematic [32]. Nevertheless, calculations of  $\mathcal{G}$  which assumed an idealized 120° dihedral angle were also

made for comparison wherein the triple-junction length is determined by fitting a third-degree polynomial to the vertex points that make up the triple junction.

The normalized integral mean curvature of the grain faces,  $\mathcal{G}$ , as a function of the number of grain faces,  $F$ , is plotted in Fig. 6. The small gray symbols represent  $\mathcal{G}$  of each individual grain in the analysis volume and the large symbols represent the average value of  $\mathcal{G}$  for all grains with that number of faces, referred to hereafter as topologically average values. Grains with  $\mathcal{G} < 0$  have a negative growth rate, while grains with  $\mathcal{G} > 0$  have a positive growth rate. Not surprisingly, the grains with the largest number of faces tend to have the fastest positive growth rates, while grains with few faces tend to have negative growth rates. It is important to note that this analysis assumes that the grain energy and mobility do not have a large effect on the curvature of the boundaries, and that they are nearly isotropic and can therefore be factored out of the integral in Eq. (1). While this is not generally true for metallic systems, the low anisotropy in body-centered cubic materials makes this a reasonable assumption, particularly when comparing the average behaviors of the ensemble of grains, where small differences are expected to be averaged out. It can be seen that  $\mathcal{G}$  is not a direct function of the number of faces of the grain (as is the case in two dimensions), but rather there is a distribution in  $\mathcal{G}$  for a given number of faces.

Also plotted in Fig. 6 is the topologically averaged  $\mathcal{G}$  using the assumption of 120° dihedral angles, as described in Eq. (3). While the general trend is repeated, with particularly good matching near  $\mathcal{G} = 0$ , there are considerable discrepancies at smaller face numbers. This is attributed to the artifacts found in the reconstruction of the triple lines (see Fig. 5c) due to the high curvatures near the triple lines and quadruple points, which are most susceptible to error. Grains with few faces tend to be the smallest grains, and thus a larger fraction of their total interfacial curvature is made of these triple lines, leading to a higher degree of

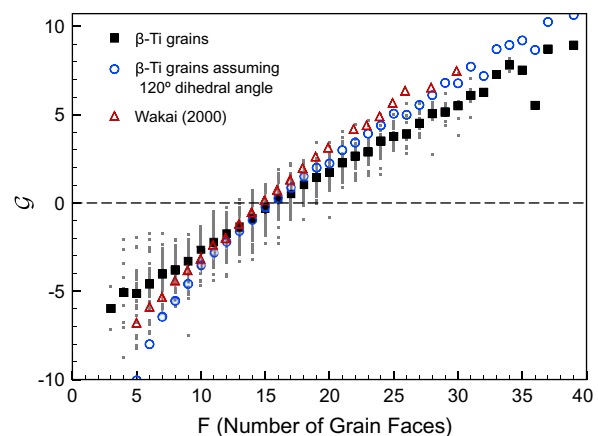


Fig. 6. The normalized integral mean curvature of the grain faces,  $\mathcal{G}$ , as a function of the number of faces,  $F$ , per grain. The small symbols represent each individual grain while the large symbols represent the average value of  $\mathcal{G}$  for each face class.

error. Another source of the discrepancy may be the assumption of isotropic triple lines; however, it is unclear why grains with fewer faces would be more prone to this error. In either case, the comparison shows the advantage of isolating the integral mean curvature of the grain faces in determining the geometric term in the growth rate.

Fig. 6 also includes the results of a vertex evolution model by Wakai et al. [6]. The Surface Evolver data closely matches the experimental results, with a similar crossover point for zero  $\mathcal{G}$ , but the overall slope of the curve is steeper in the simulation. The analysis of the Ti- $\beta$  grains showed that grains with 15.5 averaged faces have a  $G$  of zero (a grain can not actually be constructed with 15.5 faces and the fractional face is a mathematical construct to determine the zero growth condition); similarly, in the simulation by Wakai, the measured zero growth rate occurs near  $F = 15$ . Similar results have been found in 3-D liquid–gas foam networks [33], Monte Carlo simulations [34,35] and vertex models [12]. These similar results suggest that in the present materials system, the anisotropic effects of the grain boundary energy and mobility do not play a significant role, and that the geometry of the grain interfaces plays a significant role in the growth rate of the grains. However, one would expect this behavior would be significantly different in materials systems where high anisotropy terms would dominate the behavior.

A number of theories have suggested that the zero growth rate should occur for grains that have  $F \simeq 13.4$  [7,10,36]. Unlike the Cahn–MacPhearson–Srolovitz construction, these theories do not expect to make an exact prediction of the growth rate of individual grains; rather, they propose that the average behavior of a collection of irregular polyhedra resembles that of a single idealized regular polyhedra with the same number of faces. It has been suggested that a packing of regular polyhedra with approximately 13.4 faces represents the lowest surface-area-to-volume ratio for a space-filling network, and consequently that grains approximating these shapes should be stable (neither growing nor shrinking) [7,10,36,37]. This is consistent with the regular packing of space-filling objects, where it is found that the ideal surface-area-to-volume ratio occurs for a structure comprising one 12-sided polygon and one 14-sided polygon [38]. It is interesting to note that the average number of faces in the experimental data is 13.7, very close to the idealized value for the surface to volume ratio, but the measured zero growth occurs near 15.5 faces. One explanation for this difference is that the analytical theories predict the net curvature of a shape without accounting for the interactions of the nearest-neighbor grains. As will be shown, the nearest-neighbor interactions between grains are not random, and therefore may have a significant effect on predicting the growth rate of a given set of topologically averaged grains.

Fig. 7 plots the average number of faces of each grain's nearest neighbors,  $m(F)$ , vs. the number of faces per grain. Again the topologically averaged values are also plotted (dark squares). This analysis utilizes a much smaller num-

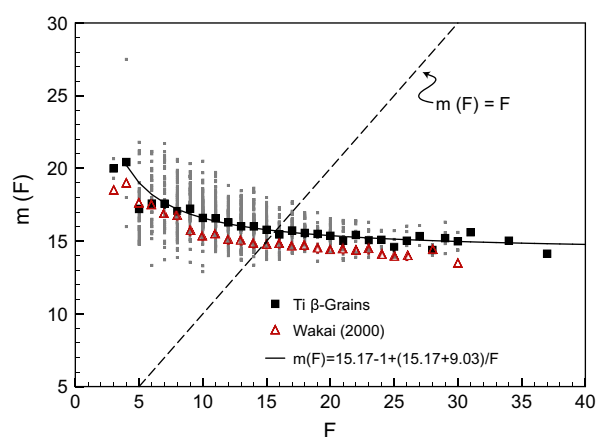


Fig. 7. Plot of the average number of faces of the nearest-neighbor grains,  $m(F)$ , vs. the number of faces of the grains,  $F$ . The dashed line represents the line along which the number of faces of a grain is equal to the average number of faces of its neighbors,  $m(F) = F$ .

ber of grains than the set of 2098 unbiased grains because here, not only must the central grain fall within the unbiased dataset, but also none of its neighbors may intersect the edges of the analysis volume, leaving 1075 grains in the nearest-neighbor analysis. This further reinforces the importance of collecting statistically large datasets if one is to examine nearest-neighbor effects on a statistical basis. The data are compared again to the Surface Evolver simulation of Wakai. For all averaged face class values, the average number of faces of the neighbors is always larger than the average number of faces for the entire system ( $\bar{F} = 13.7$ ) because, by definition, grains that have a large number of faces are counted as a neighbor more frequently. Again, a distribution in the average number of faces of a grain's neighbors is observed for a given topological class, but the average non-linear behavior is consistent with the Aboav–Weaire relation [13,39], which predicts that for a 3-D system the average number of faces of the nearest neighbor is given by:

$$m(F) = \bar{F} - 1 + \frac{\bar{F} + \mu_F}{F} \quad (8)$$

where  $\bar{F}$  is the average number of faces in the system and  $\mu_F$  is the second moment in the distribution of the number of faces in the system. The least-squares fit of this equation to all of the nearest-neighbor data is also included in Fig. 7, and shows a very close correlation to the topologically averaged data. The fit shows that  $m(F) \propto 1/F$ , but the fit coefficients of 15.17 and 9.03 do not accurately reproduce the calculated values for the average and variance, respectively, for the system ( $\bar{F} = 13.7$ ,  $\mu_F = 30.7$ ). The discrepancies in the fit values are most likely due to the assumption that the distribution in the number of faces is symmetric, whereas the experimental data clearly shows that the distribution is not symmetric (see Fig. 4). Also shown in Fig. 7 is the line  $m(F) = F$ , i.e. where the number of average nearest-neighbor faces is equal to the number of faces of the central grain. The averaged topological values

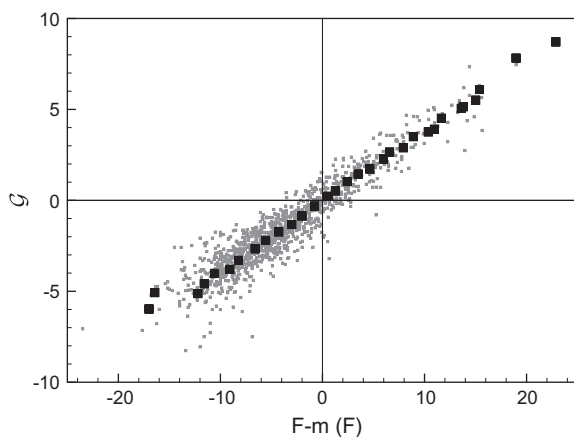


Fig. 8. Plot of the normalized integral mean curvature of the grain faces,  $\mathcal{G}$ , vs. the difference in the number of faces for a grain and the average number of faces of the grain's nearest neighbors,  $F - m(F)$ . The black squares indicate the average values for grains that have the same number of faces.

cross this line at  $F = 15.5$ , the same value that represented  $\mathcal{G} = 0$  for the topologically averaged grains (Fig. 6).

To elucidate more clearly the nearest-neighbor correlations, Fig. 8 plots  $\mathcal{G}$  as a function of  $F - m(F)$ , the difference in the number of faces of a given grain and the average number of faces of its nearest-neighbor grains. This relationship is linear and passes through the origin, which indicates that, when grains have the same number of faces as their neighbors (on average),  $\mathcal{G}$  is zero. Grains that have more faces than their neighbors tend to be growing, while grains that have fewer faces than their neighbors tend to shrink. Fig. 7 and the Aboav–Weaire relationship indicate that these correlations are not random, and grains should not be considered to exist in a mean field; rather, the topology of the grain is related to the neighborhood of the grain, which in turn affects the grain growth.

The differences between the analytical theories and the experimental findings shown in Fig. 6 are explained by the linear relationship between the grain neighborhood and the normalized integral mean curvature demonstrated in Fig. 8. The analytical theories do not consider the grains' nearest neighbors, resulting in the prediction of a zero geometric growth rate for those grains with the ideal ratio of surface area to volume (and thus the lowest magnitude integral mean curvature), at  $F \sim 13.4$ . However, as shown in Fig. 7, grains with 13–14 faces are surrounded by grains that have on average a higher number of faces. The central grains in this case would be surrounded by grains that are growing; therefore, the central grains would have a negative growth rate. Glicksman et al. have presented this as a possible explanation for the discrepancies between their analytical results and simulations [36].

It is important to note that the phenomena reported here represent the average behavior of the grains, and as such do not describe the behavior of each individual grain. However, the results do suggest that it is possible to con-

struct statistically based laws that predict the coarsening behavior of grain networks without requiring detailed information on the individual grains, as long as non-random nearest-neighbor interactions are accounted for in the predictions.

#### 4. Conclusions

This paper presents the results of a serial sectioning analysis of 2098 Ti- $\beta$  grains in Ti-21S. From the reconstruction, the 3-D grain size and number of grain faces is determined unambiguously, allowing for direct comparison to theories and simulations. It is found that the modern 3-D theories compare very well with the experimental results. Additionally, using a modified analysis of the MacPherson–Srolovitz formulation, the integral mean curvature of the grain faces of the grains was determined without requiring detailed analysis of the triple-junction geometry. These results also compare well with simulations indicating that, on average, the grains with between 15 and 16 faces should have a zero growth rate in the polycrystalline system. It is shown that this is the same number of faces for which, on average, a grain has the equivalent number of faces as its contacting neighbors. For grains with fewer than 15.5 faces, the contacting neighbors typically have more faces, and thus these grains would be expected to shrink. For grains that have more than 15.5 faces, the contacting neighbors have fewer faces, thus grains with more than 15.5 faces would be expected to grow. This analysis shows the importance of considering not only the average grain topology, but also the topology of the nearest grain neighbors when calculating grain growth rates and predicting grain coarsening phenomena. Based on this data, it is suggested that the non-random nearest-neighbor effects within the grain network play a significant role in controlling grain stability, and that the number of faces required for stability (zero growth rate) is  $\sim 15.5$ .

#### Acknowledgements

The authors greatly acknowledge the financial support of Office of Naval Research/DARPA under the D 3-D Digital Structures program. The authors also would like to thank Sukbin Lee and Anthony Rollett at Carnegie Mellon University for the generous use of the 3MC surface meshing code. D.J.R. and G.S. would also like to acknowledge extremely useful discussions with M.E. Glicksman.

#### References

- [1] Smith C. Trans Am Inst Min Metall Eng 1948;175:15–51.
- [2] von Neumann J. Metal interfaces. Cleveland, OH: American Society for Metals; 1952. p. 108–10.
- [3] Mullins W. J Appl Phys 1956;27:900–4.
- [4] Cahn J. Trans Metall Soc AIME 1967;239:610.
- [5] Fan D, Chen L. Acta Mater 1997;45:611–22.
- [6] Wakai F, Enomoto N, Ogawa H. Acta Mater 2000;48:1297–311.

- [7] Hilgenfeldt S, Kraynik A, Koehler S, Stone H. *Phys Rev Lett* 2001;86:2685–8.
- [8] Krill C, Chen L. *Acta Mater* 2002;50:3057–73.
- [9] Pande C, Rajagopal A. *Acta Mater* 2002;50:3013–21.
- [10] Glicksman M. *Philos Mag* 2005;85:3–31.
- [11] MacPherson R, Srolovitz D. *Nature* 2007;446:1053–5.
- [12] Barrales Mora L, Gottstein G, Shvindlerman L. *Acta Mater* 2008;56:5915–26.
- [13] Aboav D. *Metallography* 1970;383–90.
- [14] Palmer M, Fradkov V, Glicksman M, Rajan K. *Scripta Metall Mater* 1994;30:633–7.
- [15] Williams W, Smith C. *Trans Am Inst Min Metall Eng* 1952;194:755–65.
- [16] Smith C. *Acta Metall* 1953;1:295.
- [17] Thornton K, Poulsen H. *MRS Bull* 2008;33:587–95.
- [18] Spanos G. *Scripta Mater* 2006;55.
- [19] Uchic M. *JOM* 2006;58.
- [20] Groeber M, Ghosh S, Uchic M, Dimiduk D. *Acta Mater* 2008;56:1257–73.
- [21] Zhang C, Suzuki A, Ishimaru T, Enomoto M. *Metall Mater Trans A – Phys Metall Mater Sci* 2004;35A:1927–33.
- [22] Wall M, Schwartz A, Nguyen L. *Ultramicroscopy* 2001;88:73–83.
- [23] Spanos G, Rowenhorst D, Lewis A, Geltmacher A. *MRS Bull* 2008;33:597–602.
- [24] Rowenhorst D, Kuang J, Thornton K, Voorhees P. *Acta Mater* 2006:2027–39.
- [25] Saito T, Toriwaki J. *Pattern Recognit* 1994;27:1551–65.
- [26] Stoev S. In: *Proceedings of the 8th international conference on computer graphics, visualization, and interactive digital media (WSCG2000)*; 2000. p. 100–7.
- [27] Dillon S, Rohrer G. *J Am Ceram Soc* 2009;92:1580–5.
- [28] Zöllner D, Streitenberger P. *Scripta Mater* 2006;54:1697–702.
- [29] Pande C, McFadden G. *Acta Mater* 2010;58:1037–44.
- [30] Lorensen W, Cline H. *Comput Graph (ACM)* 1987;21:163–9.
- [31] Wu Z, Sullivan Jr J. *Int J Numer Methods Eng* 2003;58:189–207.
- [32] Glicksman M, Rios P, Lewis D. *Philos Mag* 2009;89:389–403.
- [33] Lambert J, Cantat I, Delannay R, Mokso R, Cloetens P, Glazier J, et al. *Phys Rev Lett* 2007;99.
- [34] Glazier J. *Phys Rev Lett* 1993;70:2170–3.
- [35] Streitenberger P, Zöllner D. *Scripta Mater* 2006;55:461–4.
- [36] Rios P, Glicksman M. *Acta Mater* 2008;56:1165–71.
- [37] Rivier N. *J Phys (Paris), Colloque* 1982;43:91–5.
- [38] Weaire D, Phelan R. *Philos Mag Lett* 1994;69:107–10.
- [39] Weaire D. *Metallography* 1974;7:157–60.